Molecular Vision 2014; 20:1422-1433 <http://www.molvis.org/molvis/v20/1422>
Received 6 July 2014 | Accepted 8 October 2014 | Published 10 October 2014

Developmentally dynamic colocalization patterns of DSCAM with adhesion and synaptic proteins in the mouse retina

Gabriel Belem de Andrade,[1,2] Landon Kunzelman,[3] Morgan M. Merrill,[1] Peter G. Fuerst[1,4]

[1]University of Idaho, Department of Biological Sciences, Moscow, ID; [2]CAPES Foundation, Ministry of Education of Brazil, Brasília-DF, Brazil; [3]Department of Biology, Brigham Young University, Idaho, Rexburg, ID; [4]University of Washington School of Medicine, WWAMI Medical Education Program, Moscow, ID

Purpose: The *Down syndrome cell adhesion molecule* (*Dscam*) gene is required for normal dendrite arborization and lamination in the mouse retina. In this study, we characterized the developmental localization of the DSCAM protein to better understand the postnatal stages of retinal development during which laminar disorganization occur in the absence of the protein.
Methods: Immunohistochemistry and colocalization analysis software were used to assay the localization of the DSCAM protein during development of the retina.
Results: We found that DSCAM was initially localized diffusely throughout mouse retinal neurites but then adopted a punctate distribution. DSCAM colocalized with catenins in the adult retina but was not detected at the active zone of chemical synapses, electrical synapses, and tight junctions. Further analysis identified a wave of colocalization between DSCAM and numerous synaptic and junction proteins coinciding with synaptogenesis between bipolar and retinal ganglion cells.
Conclusions: Research presented in this study expands our understanding of DSCAM function by characterizing its location during the development of the retina and identifies temporally regulated localization patterns as an important consideration in understanding the function of adhesion molecules in neural development.

The development of the retina requires the generation and integration of a large number of distinct cell types into functional neural circuits. Cells of the retina are distributed in three cellular layers: the outer nuclear layer (ONL), which contains rod and cone photoreceptors; the inner nuclear layer (INL), which consists of bipolar cells, amacrine cells, horizontal cells, and Müller glia; and the retinal ganglion cell layer (RGL), which contains amacrine cells and ganglion cells that convey photodetection to the rest of the brain [1]. Two synaptic layers, the outer plexiform layer (OPL), between the ONL and the INL, and the inner plexiform layer (IPL), between the INL and the RGL, contain the axons and dendrites that connect the cells of the retina and form the functional circuitry of vision. Members of the *Down syndrome cell adhesion molecule* (*Dscam*) gene (OMIM 602523) family are required for spacing of similar cells and for laminar organization in the mouse retina, the latter a phenotype that is shared with the chick retina, in which knockdown of DSCAM can promote disorganization of retinal neurite banding [2-4]. Although studies have revealed phenotypes that occur in *Dscam* loss and gain of function experiments, the process by which DSCAMs mediate these functions has remained elusive.

In this study, we assayed the localization of DSCAM in the developing mouse retina. We found that the DSCAM protein was initially spread diffusely throughout the neurite containing the retinal IPL, but as development proceeded, the protein became concentrated in distinct puncta. DSCAM had temporally regulated distribution to excitatory and inhibitory synapses and was also found to colocalize with catenins, proteins that anchor cadherins to the cytoskeleton and play an important role in Wnt and other types of signaling [5]. The localization pattern we characterized identifies the catenin-containing adherens junction as a novel target for future studies aimed at understanding the integration of neurons into neuronal circuits and tissues. This study also demonstrates the dynamic localization pattern of a cell adhesion molecule, suggesting differential localization as a mechanism by which a single CAM can serve multiple functions during development.

METHODS

Animal care and ethics: All protocols were performed in accordance with the University of Idaho Institutional Animal Care and Use Committee, and adhered to the ARVO statement for use of animals in research. Mice were fed ad libitum

Correspondence to: Peter G. Fuerst, Department of Biological Sciences, University of Washington WWAMI Medical Education Program, University of Idaho, Moscow, Idaho 83844; Phone: (208) 885 7512; FAX: (208) 885 7905; email: fuerst@uidaho.edu

under a 12 h:12 h light-dark cycle. Mice taken for study were deeply anesthetized with tribromoethanol (500 mg/kg). Blood was flushed out of vessels by cardiac perfusion with PBS (140 mM NaCl, 2.5 mM KCl, 1.75 mM KH_2PO_4 and 10 mM Na_2HPO_4, pH 7.4). After the cardiac perfusion, tissues were collected. Mice carrying the *Dscam*^{del17}, *Dscam*^{2J}, *Dscam*^{3J} and *Dscam*^{FD} mutations were used in this study. These do not make a DSCAM protein that is detectable with either western blot analysis or immunohistochemistry [6,7]. At least three retina sections from three different mice were imaged at each age and/or genotype for each antigen. Male and female mice were used in this study. No differences between the sexes were detected.

Genotyping: Mice were genotyped with PCR as previously described [1,3,8,9]. *Dscam*^{del17} mice were genotyped using the primers DscamF CTT TGC GCG TTA TGA TCC T and DscamR GTG GTG TCG ATA CTG ATG. DNA was amplified in a thermocycler using the following program: 94 °C 2 min, 35 cycles of 94 °C 30 s, 53.5 °C 30 s, 72 °C 25 s and then 72 °C for 2 min. This results in amplification of a product of 170 base pairs (bps) from wild type mouse DNA. The *Dscam*^{del17} mutation is a deletion mutation, resulting in a 133 bp product amplified from mice homozygous for the mutation, or both bands in heterozygotes. *Dscam*^{2J} mice were genotyped using the primers Dscam2J F GCG AGA TTA AGA ACGAAC and Dscam2J R TCC TCC TTG GTA CGG GTA using the following thermocycler program. 94 °C 2 min, 35 cycles of 94 °C 30 s, 58 °C 30 s, 72 °C 50 s, followed by a final incubation at 72 °C for 4 min. DNA amplified from mice carrying the *Dscam*^{2J} mutation will result in a PCR product 152 bps in size, while DNA prepared from wild type mice will yield no product. *Dscam*^{3J} mice were genotyped using the same primers and genotyping program that is used to genotype the *Dscam*^{del17} allele. Following PCR, 10 µl of the product is digested with the restriction enzyme BstUI (0.5 µl enzyme, 2 µl enzyme buffer and 7.5 µl water). The mutation destroys a BstUI restriction site, which cleaves the 170 bp product into two nearly equal fragments. *Dscam*^{FD} mice were genotyped using the primers GCA CCA TGA TTG ACA GCC AAG TG and TGA GGG TCA CCT ACC AGG AG. The primers were used to amplify DNA using the following program: 94 °C 2 min, followed by 38 cycles of 94 °C 20 s, 60 °C 30 s and 72 °C 70 s, concluded with a final 4 min incubation at 72 °C. Amplification of DNA from mice carrying the *Dscam*^{FD} mutation results in a product of approximately 500 bp, while no product is amplified from DNA isolated form wild type mice. Tail or toe tip biopsies were prepared for genotyping by boiling the biopsies in 25 µM sodium hydroxide and 0.2 µM EDTA for 15 min. Samples were neutralized with an equal volume of Tris Cl, pH 5.0. DNA was added to OneTaq Hot Start 2x Master Mix with standard buffer, along with primers and water to dilute the PCR mixture to 1× concentration (New England Biolabs, Ipswich, MA).

Retina dissection and staining: Eyes were carefully enucleated following cardiac perfusion and hemisected. The posterior half of the eye was incubated in 4% paraformaldehyde for 50 min on ice (DSCAM staining) or 30 min at room temperature (all other staining), followed by three washes in large volumes of PBS. Retinas were isolated from the posterior half of the eye and either dehydrated and embedded in paraffin or equilibrated in 30% sucrose for 1 h and then frozen in optimum cutting temperature (OCT). Sections were cut with a cryostat or microtome at 10 µm onto Super Frost plus charged slides (Fisher Scientific, Pittsburgh, PA, catalog number 12-550-15) slides. Paraffin sections were rehydrated and stained with hematoxylin and eosin. Frozen sections were blocked in 7.5% normal donkey serum and 0.1% Triton X-100 in PBS for 20 min (blocking solution). Primary antibodies were diluted in blocking solution and incubated overnight at 4 °C. Primary antibodies were washed three times in PBS for 10 min. Secondary antibodies were diluted in blocking solution, and 500 µl was applied over a given slide and incubated at room temperature for 2 h. Slides were then washed three times for 15 min in PBS. The second wash contained 1 µl 10 mg/ml 4',6-diamidino-2-phenylindole (DAPI) solution per 50 ml of PBS. Whole retinas were stained in a similar fashion except that the blocking solution contained 0.4% Triton, the primary antibodies were incubated over 3 to 4 days, and the secondary antibodies were incubated at 4 °C for 2 days.

Antibodies/lectins : Fluorescent secondary antibodies were obtained from Jackson ImmunoResearch (West Grove, PA) and were used at a 1:500 dilution in blocking solution. Primary antibodies details are found in the following list. Rabbit anti 14-3-3 Epsilon (ywhae; Cell Signaling Technology, Danvers, MA; 9635; 1:400), Rabbit anti 14-3-3 Eta (ywhah; Cell Signaling Technology; 9640; 1:400), Mouse anti β-Catenin (BD Biosciences San Jose, CA; 610153; 1:200), Goat anti Bassoon (Santa Cruz Biotechnology, Santa Cruz, CA; sc-18565; 1:400), Mouse anti Cadherin 8.1 (DSHB, Iowa City, IA; 1:100), Mouse anti Cask (NeuroMab, Davis, CA; 75-000; 1:400), Mouse anti Connexin 36 (Millipore, Darmstadt, Germany; MAB3045; 1:400), Mouse anti Connexin 45 (Invitrogen, Franklin Lakes, NJ; 415 800; 1:400), Mouse anti CTBP2 (BD Biosciences; 612042; 1:400), Goat anti DSCAM (R&D Systems Minneapolis, MN; AF3315; 1:500 for WBA, 1:100 for IHC), Rabbit anti GABAa receptor delta subunit 2 (Synaptic Systems, Göttingen, Germany; 224 003; 1:400), Mouse anti Gap43 (Millipore; MAB347; 1:400), Mouse anti GluR1 (NeuroMab; 75-327; 1:500), Mouse anti

GluR2 (NeuroMab; 75-002; 1:400), Rabbit anti GluR4 (Cell Signaling Technologies; 8070; 1:400), Goat anti GluR5 (Santa Cruz Biotechnology; Sc-7616; 1:100), Mouse anti GlyR (Synaptic Systems, Göttingen, Germany; 146 011; 1:400), Mouse anti ß-protocadherin (NeuroMab; 75-185; 1:400), Rabbit anti Magi2 (Sigma-Aldrich, St. Louis, MO; HPA 013 650; 1:400), Rabbit anti Magi3 (Sigma-Aldrich; HPA 007 923; 1:400), Mouse anti Mitochondria (Ox Phos; Life Technologies; A21348; 1:750), Rat anti N-Catenin (DSHB, IA; 1:200), Mouse anti Neuroligin 1 (NeuroMab; 75-160; 1:400), Rabbit anti NMDA 2AB (Millipore; AB1548; 1:400), Rabbit anti NMDA 2b (NeuroMab; Q00960; 1:400), Mouse anti NR1 (NeuroMab; 75-272; 1:500), Rabbit anti P2X2 (Alomone labs, Jerusalem, Israel; APR-003; 1:100), Rabbit anti P2X7 (Millipore; AB5246; 1:100), Mouse anti PSD95 (NeuroMab; 75-028; 1:200), Rat anti R-Cadherin (MRCD5; DSHB; 1:200), Rabbit anti Rim2 (Synaptic System; 140 103; 1:400), Mouse anti Sap102 (NeuroMab; 75-058; 1:200), Mouse anti Shank (NeuroMab; 75-089; 1:400), Rabbit anti Synapsin (Cell Signaling Technology; 5297; 1:400), Mouse anti synaptotagmin2 (ZIRC, Eugene, OR; 1:500), Mouse anti Syntaxin I (Sigma-Aldrich; S 0664; 1:1000), Rabbit anti Syntaxin II (Synaptic Systems; 110-022; 1:200), Rabbit anti Syntaxin III (Novus Biologicals, Littleton, CO; AB4113; 1:1000), Rabbit anti Syntaxin IV (Millipore; AB5330; 1:200), Rabbit anti ZO-1 (Invitrogen; 61-7300; 1:400), Rabbit anti ZO-2 (Invitrogen; 71-1400; 1:400) and Rabbit anti ZONAB (Invitrogen; 48-2800; 1:400. Secondary antibodies were purchased from Invitrogen (all Ig subtype specific antibodies) or Jackson ImmunoResearch (all other secondary antibodies) and used at a dilution of 1:1000.

Cell culture: Retinas from P0 mice were isolated in Dulbecco's modification of Eagles Media/F12 (DMEM/F12) and incubated in TrpleE (Invitrogen) and incubated in TrplE (Invitrogen) for 20 min at 37 °C. After 20 min, the retinas were gently triturated into large clumps of cells and incubated for an additional 20 min. A second round of trituration was performed until the cells were dispersed into single cells or small clumps. Cells were plated on coverslips treated with poly-d-lysine, laminin, and fibronectin in neurobasal media supplemented with B27 (Custom) and N2 at 1× concentrations (all reagents from Invitrogen). Cells were incubated at 37 °C 5% CO_2 for 2 weeks after which the cells were fixed in 4% buffered paraformaldehyde (PFA; Electron Microscopy Sciences, Hatfield, PA) supplemented with 12% sucrose for 10 min at 37 °C. The coverslips were then washed with PBS and stored at 4 °C until staining.

Colocalization analysis: Twenty µm retina sections were stained with antibodies to DSCAM and a second protein. Thirty confocal slices were imaged every 0.3 µm using an Olympus Fluoview confocal microscope (Tokyo, Japan) microscope. Images were opened in FIJI and prepared for analysis by cropping the IPL, applying a 1 pixel median filter for noise reduction, and then changing each channel's contrast and brightness to set equal puncta intensity and threshold for background subtraction. Images were analyzed for colocalization using custom software as previously described [10]. Briefly, thirty confocal images were collected for each pair of antigens compared. The degree of colocalization between different channels is measured. One of the two channels is rotated 180 degrees along the vertical axis (so as to maintain distribution of staining along S1-S5 of the inner plexiform layer) as a control. This software was developed by the research group of R.O. Wong and refined by A. Bleckert [11]. As a control, one of the two channels was flipped along the vertical axis, to randomize the distribution of the staining while maintaining any gradients of stain distribution within the inner plexiform layer.

Colocalization analysis: To evaluate the frequency of DSCAM colocalization with other proteins, confocal images were first collected using an Olympus Fluoview 1000 microscope at 1200× total magnification. Sections from the retinas of three independent mice were imaged at each specified age. Areas of the images in which staining of synaptic markers was not present, as the result of blood vessels, tissue tear, or glial processes, were outlined in Adobe Photoshop. The background of the image was set to black to eliminate dim background staining, leaving immunofluorescence associated with DSCAM or other puncta. The DSCAM or other protein puncta were counted. In this case, DSCAM was imaged in the red channel while the other protein was imaged in the green channel. To account for differences in the size of the puncta, the number of times a red punctum overlapped at least 50% with a green punctum was counted, as was the number of times a green punctum overlapped at least 50% with a red punctum. These numbers were used to generate the percentage of puncta that overlapped, reported in Table 1. As a control, the staining in the green channel was flipped along the vertical axis, therefore randomizing the relationship between the stains. The green puncta were counted again, and any that fell on areas that had been previously outlined in which no synaptic staining occurred were excluded, because otherwise the presence of blood vessels and other areas lacking staining would artificially decrease the chance of random colocalization, which cannot occur in an area where no synaptic staining was present in the first place. Likewise, areas that did not have synaptic staining were flipped to identify the number of red puncta onto which no green puncta could fall. The red and green puncta that overlapped

Table 1. Table of colocalization.

Antigen	Age	Colocalization		Flipped	
		R/G	G/R	R/G	G/R
SAP102	P7	6.7%	6.3%	4.1%	2.6%
SAP102	P14	11.3%	5.6%	5.6%	2.6%
SAP102	Adult	11.6%	6%	4%	2%
β-catenin	P14	21.5%	13.1%	6.7%	2.6%
GABAaδ2	P14	10.8%	5.9%	8.3%	3.3%
GAP43	P14	4.2%	3.6%	4.4%	3.3%
GluR4	P14	25.5%	6.4%	9.3%	4.3%
MAGI2	P14	5.6%	8.2%	2.4%	3.9%
α-n-catenin	P14	24.1%	10.4%	5.9%	3.2%
γ-protocadherin	P14	20.3%	8%	7.7%	2.7%
RIM2	P14	17.0%	4.2%	10.7%	2.9%
Syntaxin3	P14	7.5%	4.7%	3.9%	3.1%

by 50%, counted independently, were counted again and used to calculate the percentage overlap. To compare the number of colocalized puncta with the number of randomly colocalized puncta, the number of randomly colocalized puncta was divided by the ratio of the flipped red or green puncta and the total number of red or green puncta, which increased the count of randomly colocalized puncta and corrected for the decrease in potential random colocalization caused by the presence of areas that did not contain synaptic staining.

Imaging: Sections and whole retinas were imaged using either an Olympus spinning disk (DSU) confocal microscope or an Olympus Fluoview confocal microscope. Images were cropped and rotated using Adobe Photoshop software. Any changes in brightness or contrast were made across entire images.

RESULTS

DSCAM prevents a cell type-specific adhesion that occurs in the absence of the protein. Functions for the protein in development of synapses in the mouse IPL have not been reported. Data from the chick retina and other parts of the mammalian nervous system indicate that *Dscam* is required for lamination of retinal processes and morphology of other central nervous system (CNS) neurons [2,12,13]. To determine if mouse *Dscam* plays a role in synaptic organization and to understand how a single protein can mediate such a wide range of processes, we sought to identify the dynamics of DSCAM distribution in the retina.

To understand how DSCAM mediates retinal development, we first compared the distribution of DSCAM with the development of the wild-type and *Dscam* null retina. We observed that DSCAM was diffusely spread throughout the IPL early during development of the mouse retina but by postnatal day 2 (P2) the protein began to be restricted to the puncta (Figure 1A,B). Diffuse staining transitioned to an increasingly punctate pattern as development progressed (Figure 1C,D). A similar staining pattern was observed in the adult retina (Figure 1E). Localization of residual DSCAM protein, when present, was also assayed in an allelic series of *Dscam* mutants. Residual DSCAM protein was observed aggregated around the cell soma of the $Dscam^{del17}$, $Dscam^{3J}$, and $Dscam^{FD}$ retina (Figure 1F,H,I). No protein was detected in the $Dscam^{2J}$ retina, as previously described (Figure 1G) [6]. Antibody specificity was assayed in the adult retina by using a secondary-only control (Figure 1J). Organization of the wild-type and *Dscam* mutant retina was also assayed during early postnatal development (Figure 1K–O). The wild-type and *Dscam* mutant retina appeared similar until P4, when an increase in the number of cell bodies in the inner plexiform layer was observed (Figure 1K–M). Increasing disorganization of the *Dscam* mutant retina was observed after P4 (Figure 1N,O). Therefore, during the early stages of retinal development, DSCAM was diffusely distributed, while at later developmental stages, during which the retina became disorganized in the absence of *Dscam*, the staining transitioned to a more punctate pattern.

The punctate pattern of DSCAM localization was reminiscent of the staining observed when synaptic markers are assayed. DSCAM has been implicated in synaptic lamination and receptor clustering, which suggested the protein might be localized at synapses [2,14]. Studies were conducted to identify proteins near or that colocalize with DSCAM to

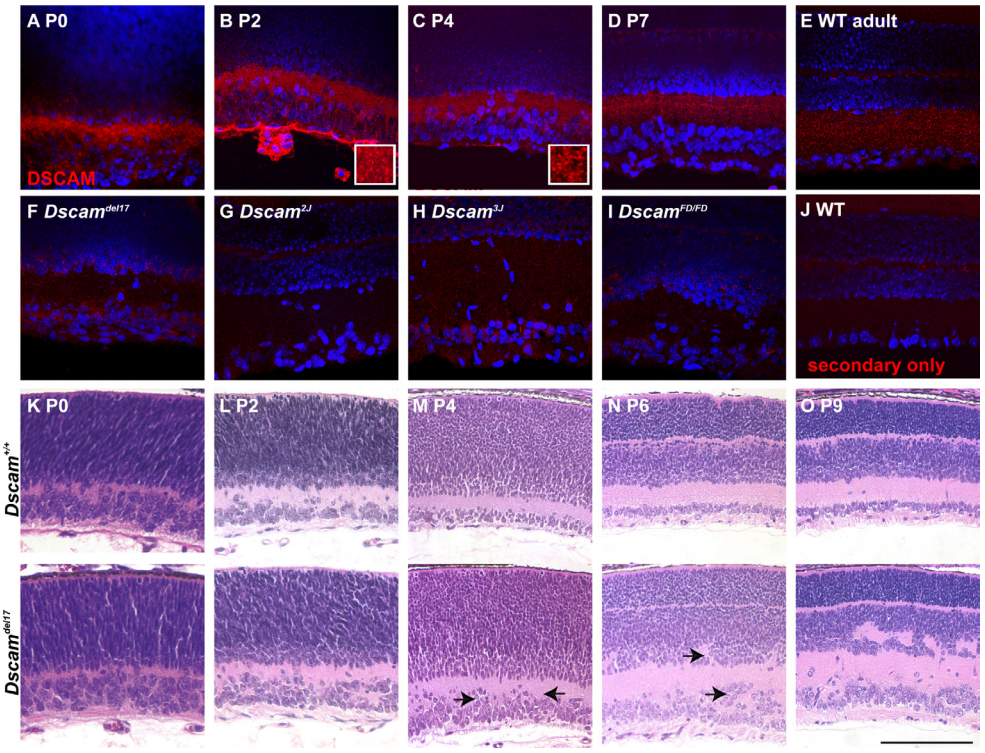

Figure 1. Localization of DSCAM in the mouse retina. **A**–**D**: Sections of wild-type retina from P0, P2, P4, and P7 mice were stained with antibodies to DSCAM. The DSCAM protein was observed throughout the inner plexiform layer (IPL) at P0 and P2. By P4, and especially by P7, DSCAM immunoreactivity was more punctate compared to earlier ages. **E**: DSCAM was observed throughout the IPL and in a limited fashion in the outer plexiform layer (OPL) of the adult retina. **F**: Residual DSCAM protein in the *Dscam*^{del17} allele accumulated around the cell soma. **G**: The DSCAM protein was not observed in the *Dscam*^{2J} allele. **H** and **I**: The DSCAM protein in the *Dscam*^{3J} and *Dscam*^{FD} alleles aggregated around the cell soma. **J**: A secondary antibody-only control demonstrated the lack of nonspecific labeling by the secondary antibody. **K**–**O**: Sections of the wild-type and *Dscam*^{del17} retina were stained with hematoxylin and eosin. Disorganization of the *Dscam*^{del17} retina became apparent by approximately P4, when cells were observed in the inner plexiform layer (arrows) and the retinal ganglion cell layer was thicker compared to wild-type (**G**; arrows) and was easily observable by P6, when uneven lamination of the retinal ganglion and inner nuclear layer was observed (**H**; arrows). The scale bar in (**I**) is equivalent to 134 µm in **A**–**J**, 91 µm in **K**, 116 µm in **L**, 170 µm in **M** and **N**, and 156 µm in **O**. The insets in **B** and **C** are 3.2 µm wide.

better assess its role in synaptic organization. Double labeling with the synaptic markers PSD95 and bassoon, markers of excitatory and inhibitory synapses, respectively, indicated a surprisingly small degree of overlap between DSCAM and these synaptic markers in the early postnatal (P7) and adult retina, which could reflect the absence of DSCAM from these foci or that the protein is not detectable at synapses (Figure 2A–C).

Some coincident localization can be expected when assaying fluorescent markers. Therefore, the degree of colocalization was assayed using customized software that measures the degree of colocalization compared to the same images in which one channel is flipped 180 degrees along the vertical axis, which preserved the gradient of immunoreactivity across the inner plexiform layer and provided control of incidental colocalization, given the degree of staining in each section [10]. In this analysis, a confocal stack of 30 sections along the Z plane of the inner plexiform layer was imaged and analyzed for each antibody pair. The colocalization analysis plotted the amount of each protein localized at different inner plexiform strata along with the degree of colocalization between the assayed proteins. Colocalization of two DSCAM antibodies was performed as a test of antibody specificity and to give a readout for near total colocalization (Figure 2D). Colocalization was plotted according to the inner plexiform layer depth compared to the flipped control (Figure 2D), with the intensity of colocalization revealed by the size of the bars projecting across the x-axis. Higher degrees of colocalization were color coded from high (red) to none (dark blue). To verify that this method was sufficient to detect colocalization of proteins that may be close together but in separate cells, such as pre- and postsynaptic proteins, we tested whether we could detect colocalization of pre- and postsynaptic markers with partial overlap. Bassoon (presynaptic at GABAergic and glycinergic synapses) and the GABAa∂2 receptor, a subunit localized to all retinal GABAergic receptors, were colocalized, even in the presence of glycinergic synapses in which bassoon, but not GABAa∂2, was present [15,16] (Figure 2E). To confirm that the analysis would not give false-positive results that may occur because of the large number of synapses in the inner plexiform layer, we assayed abundant inhibitory and excitatory markers. Colocalization was not

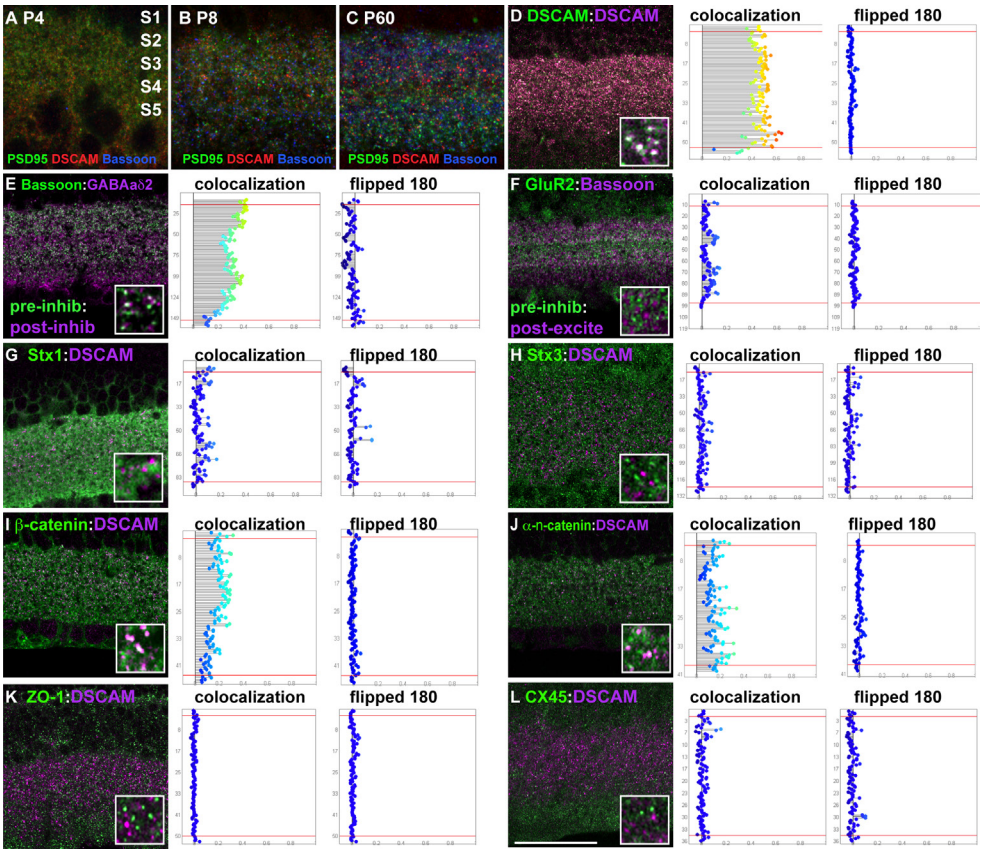

Figure 2. DSCAM colocalizes with catenins in the adult retina. **A-C**: Sections of retina were stained with antibodies to DSCAM, PSD95 and bassoon. DSCAM staining appeared to overlap minimally with synaptic markers. **D**: Retinal sections were stained with two different antibodies to DSCAM. Colocalization of markers was apparent in white (inset box). A bar chart readout of the colocalization by laminar depth, running from S1 (top) to S5 (bottom). The degree of protein colocalizing is indicated by the length of bar on the x-axis. Flipped controls were generated by rotating one of the channels 180 degrees across the vertical axis (so as to preserve S1-S5 but provide a randomized control). **E**: Retinal sections were stained with antibodies to bassoon and GABAa∂2. Colocalization of markers was apparent in white and in the bar chart (inset box). **F**: Retinal sections were stained with antibodies to GluR2 and bassoon. No colocalization of markers was apparent in white (inset box), and as depicted in the bar chart. **G**, Retinal sections from adult mice were stained with antibodies to Syntaxin1 and DSCAM. Minimal colocalization of markers was apparent (inset box) and in the bar charts. **H**: Retinal sections from adult mice were stained with antibodies to Syntaxin3 and DSCAM. No colocalization of markers was apparent in white (inset box) and as depicted in the bar charts. **I**: Retinal sections from adult mice were stained with antibodies to the adherens junctions marker ß-catenin and DSCAM. Colocalization of markers was apparent in white (inset box) and in the bar charts. **J**: Retinal sections from adult mice were stained with antibodies to the adherens junctions marker α-n-catenin and DSCAM. Colocalization of markers was apparent in white (inset box) and in the bar charts. **K**: Retinal sections from adult mice were stained with antibodies to the junction marker Zonula Occludens-1 and DSCAM. No colocalization of markers was apparent in white (inset box) or as depicted by the bar charts. **L**: Retinal sections from adult mice were stained with antibodies to the gap junction marker Connexin 45 and DSCAM. No colocalization of markers was apparent in white (inset box) or by the bar charts. The scale bar in (**A**) is equivalent to 12.5 µm in **A**, 18.9 µm in **B** and **C**, 53.25 µm in **D**-**L** and 7.9 µm in the insets from **D**-**L**.

detected when we assayed abundant inhibitory synaptic markers such as bassoon and abundant excitatory markers such as GluR2, which confirmed the specificity of the assay (Figure 2F).

Colocalization analysis was performed on a large number of synaptic markers and DSCAM in the adult retina. DSCAM was not observed in the adult retina at points labeled with a marker of conventional synapses, syntaxin 1 (Figure 2G), ribbon synapses, labeled with an antibody to syntaxin 3, and other synaptic markers [17] (Figure 2H). The lack of detectable DSCAM at synapses in the adult suggested that visible DSCAM protein was localized to other features of inner plexiform layer neurites. We therefore tested whether DSCAM was colocalized with junction markers. DSCAM was colocalized with a subset of foci that immunostained for β and α-n-catenin (Figure 2I,J). We tested whether DSCAM colocalized with markers of electrical synapses or tight junctions, which often share subunits and contain catenins. We did not observe colocalization of DSCAM with components of electrical synapses (Figure 2K,L). DSCAM was also not colocalized with markers of other synaptic and cellular compartments, including Ctbp2, NR1, synapsin, neuroligin1, NMDA2A/B, Sap102, Shank PX2X, P2X7, GluR4, GABAaδ2, CASK, bassoon, vglut3, syntaxin2, Rim2, Glycine receptors, GluR1, OxPhos (mitochondria),

MAGI2, connexin 36, 14-3-3 epsilon, syntaxin4 ZONAB, MAGI3, ZO-2, or 14-3-3 eta (Figure 3A–BB). We also tested if DSCAM colocalized with synapses in primary cultures of retinal ganglion cells, where the labeling of neurites and synapses is more distinct. Colocalization of DSCAM and synaptic markers was only rarely detected (Figure 3 CC; arrow, DD and data not shown). Therefore, in the adult retina, we observed DSCAM colocalized with a subset of catenin-containing complexes, but DSCAM did not visibly colocalize with other synaptic and adhesion molecules in the adult mouse retina.

Synaptogenesis occurs early in the postnatal mouse retina. Initially between P3 and P8, most synaptogenesis occurs between amacrine and ganglion cells. Later, starting around P9–P10, bipolar cells start to make synapses with amacrine and ganglion cells, with eye opening and visual function initiating at P13–P14. We considered that we did not observe DSCAM localization to synapses because the protein was excluded from the developing synapses as part of the maturation process or because we did not assay at an appropriate time. We therefore assayed DSCAM localization in the developing retina. Using PSD95 as a marker of excitatory synapses, developmental colocalization was assayed at P4,

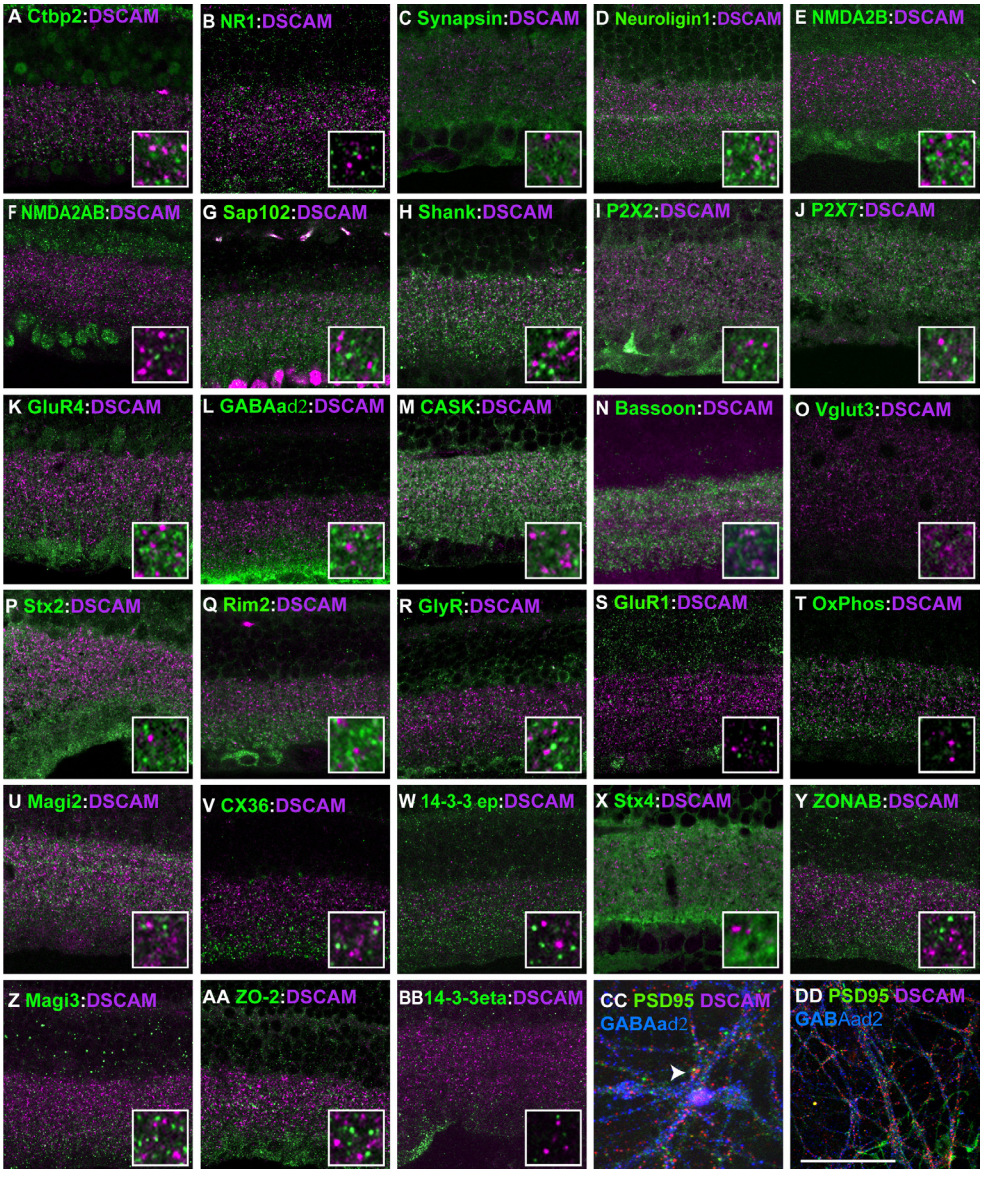

Figure 3. Limited colocalization of DSCAM and synaptic markers detected in the adult retina. Analysis of colocalization between DSCAM and C-Terminal Binding Protein-2 (CTBP2; **A**), NMDA R1 (NR1) (**B**), Synapsin (**C**), Neuroligin (**D**) NMDA 2B (**E**), NMDA 2AB (**F**) Synapse Associated Protein 102 (SAP102; **G**), Shank (**H**), P2X2 (**I**), P2X7 (**J**), Glutamate Receptor 4 (GluR4; **K**), GABAaδ2 (**L**), Calcium/Calmodulin-Dependent Serine Protein Kinase (CASK; **M**), Bassoon (**N**), Vesiclar Glutamate Transporter 3 (vglut3; **O**), Syntaxin 2 (**P**), RIM 2 (**Q**), Glycine Receptor (**R**), Glutamate Receptor 1 (GluR1; **S**), Oxidative Phosphorylation marker (**T**), Membrane Associated Guanylate Kinase 2 (MAGI2; **U**), Connexin 36 (**V**), 14-3-3 ε (**W**), Syntaxin 4 (**X**), ZO-1-Associated Nucleic Acid-Binding Protein (ZONAB; **Y**), Membrane Associated Guanylate Kinase 3 (MAGI3; **Z**), Zonula Occludens-2 (**AA**) or 14-3-3 ξ (**BB**). **CC** and **DD**, Dispersed cultures of retinal ganglion cells were stained with antibodies to DSCAM, PSD95 and GABAa∂2. Only rare examples of DSCAM overlap with synaptic markers were observed (**CC** arrow). The scale bar in **DD** is equivalent to 53.25 µm in **A** - **CC** and 7.9 µm in insets from **A** - **CC**. The scale bar in **DD** is equivalent to 15.8 µm in **CC** and 35.5 µm in **DD**.

P7, P10, and P14 and in the adult (Figure 4). Although only minimal overlap between DSCAM and PSD95 was observed at P4 or P7 (Figure 4A,B) or in the adult retina (Figure 4E), strong colocalization was observed at P10, P12 (not shown), and P14 (Figure 4C,D). A similar pattern of developmental colocalization was observed for other synaptic markers, including SAP102 (Figure 5A).

To further assay developmental colocalization, an independent method of colocalization was used. Retina sections were stained with DSCAM and the synaptic marker SAP102 and then imaged. Regions that did not contain synapses, such as blood vessels or freeze artifacts, were marked and excluded from analysis. The number of DSCAM- and SAP102-positive puncta and the number of puncta that overlapped by at least 50%, were counted at P7 and P14 and in the adult (Table 1). We repeated this analysis on nine additional markers at P14 to determine how often DSCAM colocalizes with different markers (Table 1).

We assayed a subset of these markers during development to determine if an increase in colocalization was common apart from SAP102 and PSD95. Developmental colocalization of DSCAM and GluR2 and GABAaδ2 and γ-protocadherin was detected (Figure 5B–D and data not shown). Colocalization of DSCAM and γ-protocadherin was observed at

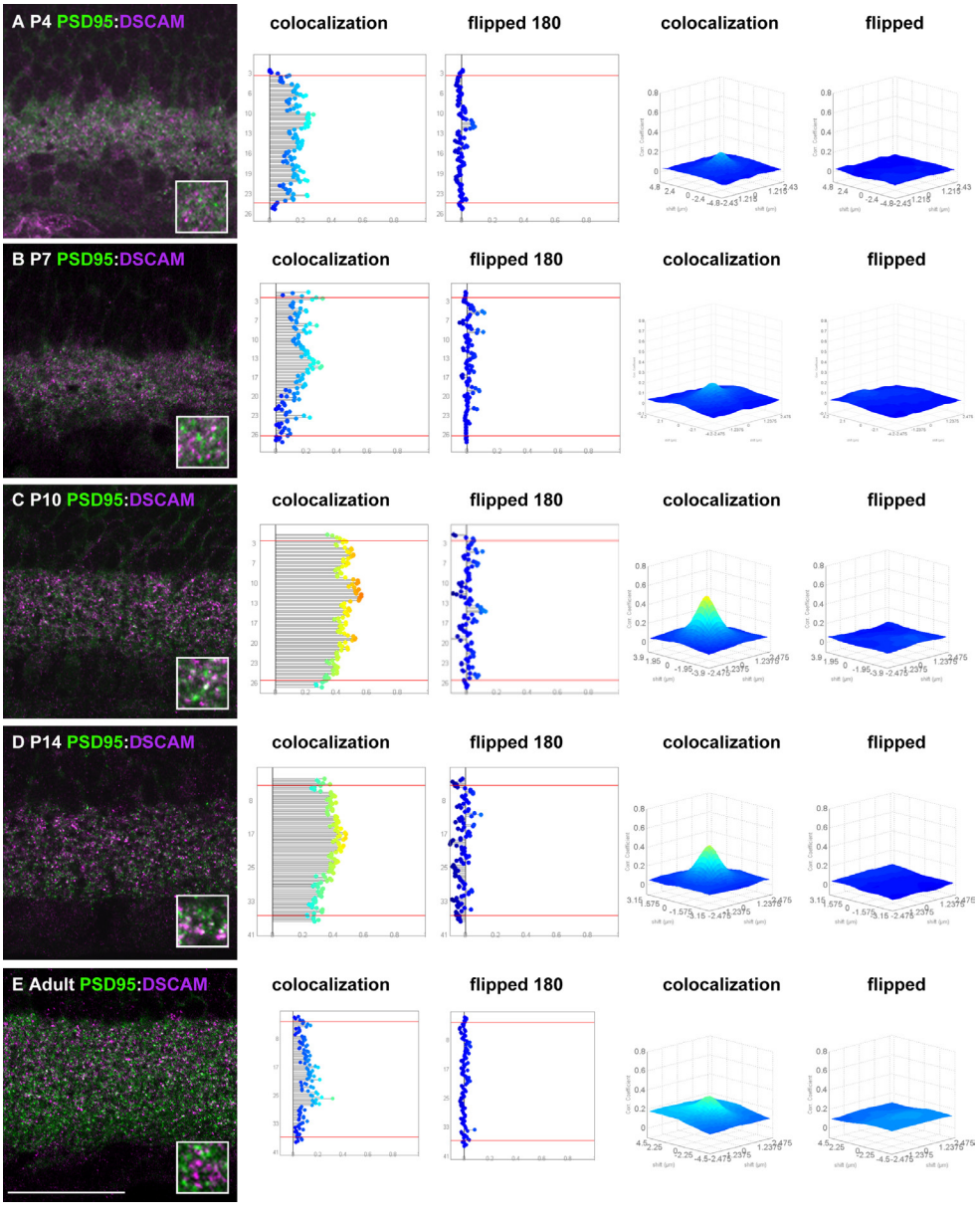

Figure 4. Robust wave of developmental colocalization between DSCAM and PSD95. **A**–**E**: Sections of the P4, P7, P10, P14, and adult retina were stained with antibodies to DSCAM and PSD95. Colocalization was plotted regarding the laminar depth and as a volcano plot. Flipped controls were generated by rotating one of the channels 180 degrees across the vertical axis (to preserve S1–S5 but provide a randomized control). The use of the flipped controls maintained the degree of immunoreactivity and provided a measure of incidental colocalization. Limited colocalization between DSCAM and PSD95 was observed at P4 (**A**) and P7 (**B**) and in the adult retina (**E**). At P10 and P14, many instances of overlap between PSD95 and DSCAM were observed (**C** and **D**) while colocalization analysis identified a higher degree of colocalization compared to flipped controls or earlier and later time points. The scale bar in **E** is equivalent to 53.25 µm in **A**–**E** and 7.9 µm in insets from **A**–**E**.

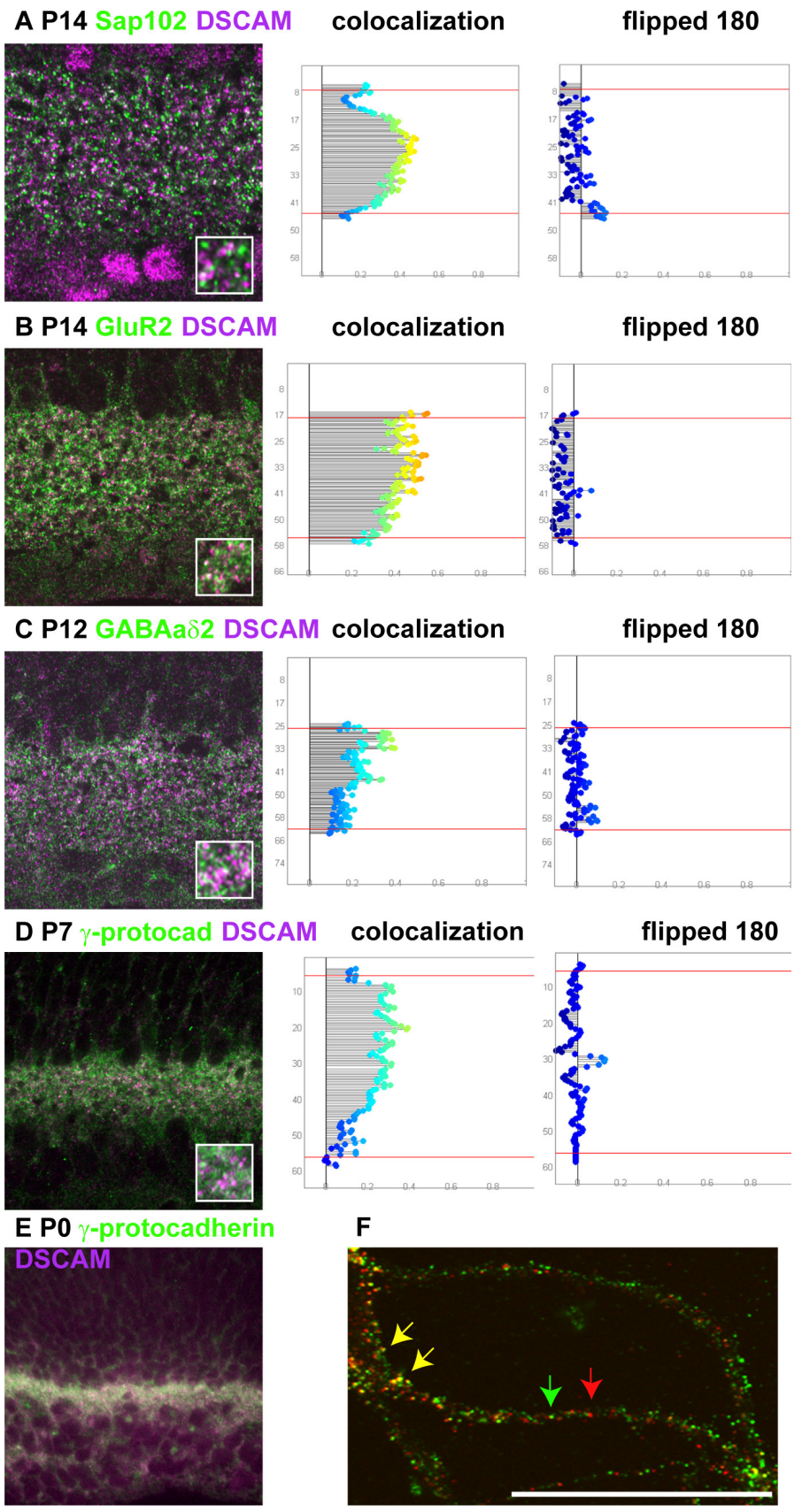

Figure 5. Developmental colocalization between DSCAM and synaptic and scaffolding molecules. **A**–**D**: Retina sections at early postnatal stages were stained with antibodies to DSCAM and Sap102 or GluR2 or GABAaδ2 or γ-protocadherin. Flipped controls were generated by rotating one of the channels 180 degrees across the vertical axis (to preserve S1–S5 but provide a randomized control). The use of flipped controls maintained the degree of immunoreactivity and provided a measure of incidental colocalization. Compared to the flipped controls, an increase in colocalization of all antigens and DSCAM was observed. **E**: Section of the P0 retina stained with antibodies to DSCAM and γ-protocadherin. Both proteins overlapped in a diffuse pattern across the inner plexiform layer. **F**: Primary culture of retinal ganglion cells stained with antibodies to DSCAM and γ-protocadherin. Overlap was observed in some but not all puncta (yellow arrows; overlap, red or green arrow; no overlap). The scale bar in (**F**) is equivalent to 53.25 µm in **A**–**D** (insets are 7.9 µm), 100 µm in **E**, and 5.17 µm in **F**.

early developmental time points, when both proteins have a diffuse localization pattern (Figure 5E). These proteins were also observed to colocalize through development and in the primary culture of retinal ganglion cells (Figure 5F). Early colocalization, by P2, was observed between DSCAM and α-n-catenin and β-catenin (data not shown).

To assay whether *Dscam* is required for the placement of synaptic or adhesion proteins, we stained sections of wild-type and *Dscam* mutant retina with antibodies to synaptic or adhesion proteins. Differences in the distribution of synaptic and adhesion markers within the inner plexiform layer were not detected when we visually compared the wild-type and *Dscam* mutant retina (Figure 6).

DISCUSSION

DSCAM in the vertebrate retina acts to regulate developmental cell death, to prevent adhesion in a large number of spatially overlapping cell types in the mouse, and to mediate neurite targeting to specific depths of the IPL in the chick retina. To better understand how DSCAM contributes to these processes, we assayed its localization during development. We found that DSCAM was broadly distributed throughout the developing and adult mouse IPL. The diffuse localization of DSCAM during early stages of retinal development and the continuous distribution throughout the IPL of the adult suggests that DSCAM would make a poor candidate to target processes to a given layer of the IPL in the mouse and that other factors might mediate this function. Localization of DSCAM in the chick retina is more limited in distribution than in the mouse and macaque, with DSCAM localization limited to a narrow band abutting the retinal ganglion cell layer [2]. The more limited localization of DSCAM in the chick retina has made identifying the role of DSCAM more amenable to loss and gain of function studies, which clearly demonstrate a role in neurite lamination [2].

To further address the function of DSCAM in the mouse, we assayed developmental localization and colocalization. During early stages of development, DSCAM was broadly distributed, after which the localization of DSCAM was observed at synaptic and catenin-containing complexes (Figure 7A). During early postnatal development, before DSCAM was observed at synapses in this study, ectopic cell type-specific adhesion occurred in the *Dscam* null retina (Figure 7B). Early diffuse localization of DSCAM and colocalization with catenins and γ-protocadherin suggest that DSCAM initially functions at adherens junctions to prevent

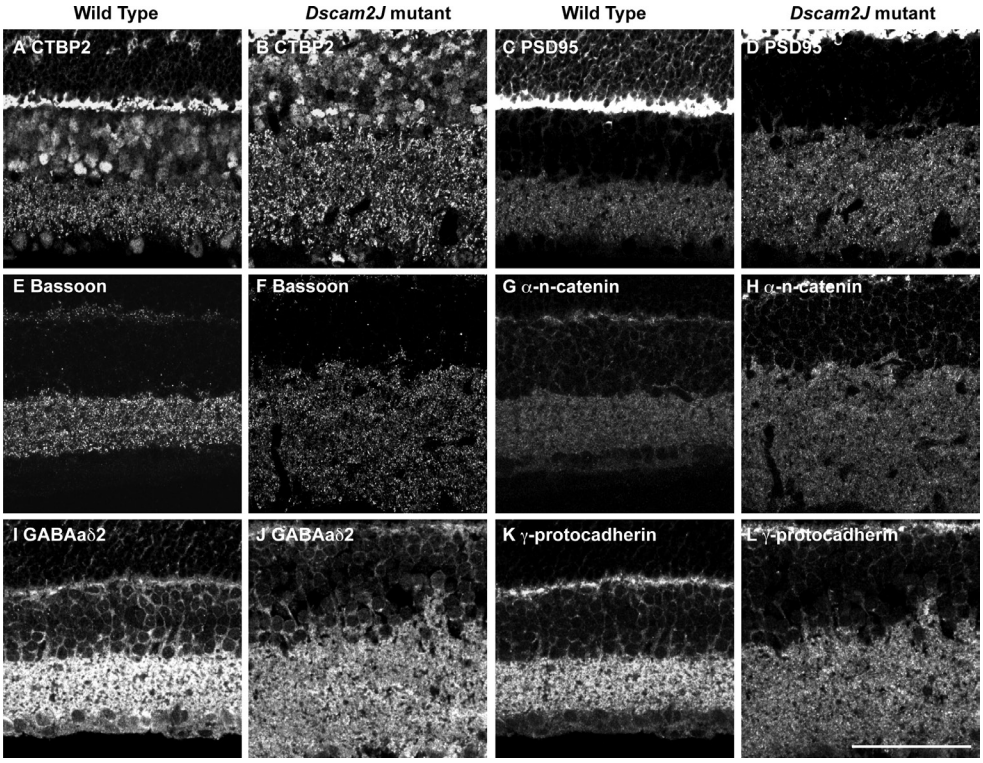

Figure 6. Synaptic and adhesion molecules in the wild-type and *Dscam* mutant retina. Wild-type and *Dscam* mutant retina sections were stained with antibodies to synaptic or junction molecules. **A** and **B**: Section of wild-type and *Dscam* mutant retina were stained with antibodies to CTBP2. **C** and **D**: Sections of wild-type and *Dscam* mutant retina were stained with antibodies to PSD95. **E** and **F**: Sections of wild-type and *Dscam* mutant retina were stained with antibodies to Bassoon. **G** and **H**: Sections of wild-type and *Dscam* mutant retina were stained with antibodies to α-n-catenin. **I** and **J**: Sections of wild-type and *Dscam* mutant retina were stained with antibodies to GABAaδ2. **K** and **L**: Sections of wild-type and *Dscam* mutant retina were stained with antibodies to γ-protocadherin. A similar distribution of synaptic markers, considering the disorganization of the *Dscam* mutant retina, was observed in the genotypes. Scale = 53.25 μm.

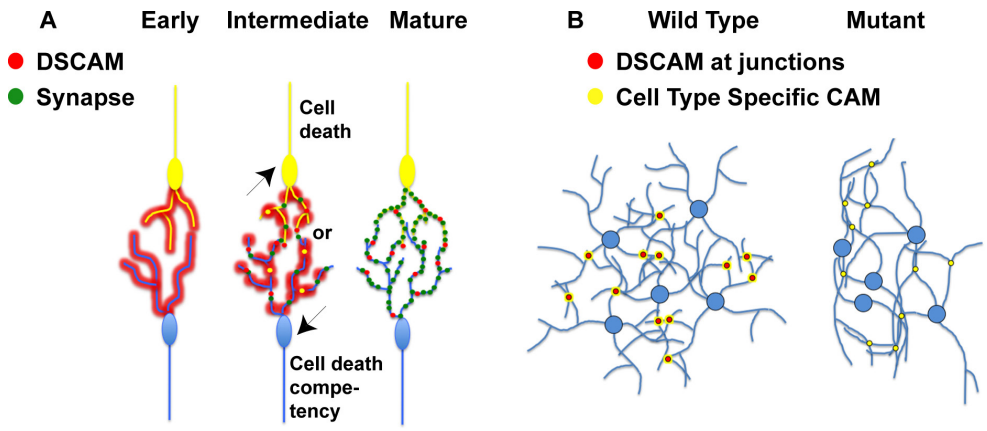

Figure 7. Model of DSCAM dynamic localization. **A**: At early developmental time points, DSCAM was localized along the developing neurites. As development proceeded, DSCAM took on a punctate pattern and overlapped with synaptic markers at time points consistent with synaptogenesis, but after ectopic adhesions had developed. As the retina matured, DSCAM was not observed overlapping with synapses but was observed overlapping with catenins. **B**: DSCAM prevented adhesion, but in the absence of the protein, other factors, possibly cadherins or other CAMs such as sidekicks, caused similar cells and their neurites to adhere to each other.

excessive adhesion. Retinal neurons express numerous cell adhesion molecules and initially have a bushy distribution, suggesting that DSCAM could function to reduce misplaced connections between retinal neurons that would result from their early bushy distribution [18,19]. At later time points, after the distribution of the retinal neurites had been refined, the DSCAM protein was observed to colocalize with synaptic markers. The timing at which DSCAM overlaps with synaptic markers coincides with the development of synaptic connections between bipolar cells and retinal ganglion cells, both of which express *Dscam*. The later decrease in DSCAM immunoreactivity at these sites could reflect its absence at these sites or that the protein is simply not detectable at later time points. Assaying the function of DSCAM at the synapse is complicated by the decrease in developmental cell death that occurs in the *Dscam* null retina and the known synaptic defects that occur in the absence of cell death pathway proteins [20]. Future studies in which conditional targeting of *Dscam* is performed after cell death has occurred but before the colocalization observed in this study are planned to overcome this challenge.

DSCAM colocalization with catenins was detected in the developing and adult retina, suggesting that the protein's activity at these foci promotes developmental cell death and prevents the ectopic clustering of cells observed in the *Dscam* mutant retina. Catenins serve to connect transmembrane cadherins with the cytoskeleton and play important developmental roles in migration, axon path finding, synapse maturation, and synapse stability, and defects in lamination of the mouse retina in the absence of β-catenin have been reported [21-23]. The identification of DSCAM at the adherens junctions suggests that cadherins are good candidates for mediating the adhesion observed in the absence of DSCAM, and the expression of some cadherins in specific types of retinal neurons suggests that cadherins may also act as cell type-specific identifiers by which like cells are spaced in horizontal mosaics across the retina [24]. Recent studies further demonstrate the importance of cadherins in laminar targeting by bipolar cells, consistent with the adherens junction being a critical site of developmental regulation [25]. Dissociation of catenin/cadherin complexes is mediated by receptor tyrosine kinases, such as Fyn. DSCAM has been shown to activate this kinase and induce growth cone collapse in axons, consistent with the increased adhesion that occurs in the absence of DSCAM and suggesting a mechanism for the adhesion observed in the *Dscam* mutant retina [26].

ACKNOWLEDGMENTS

This research was supported by the National Eye Institute Grant EY020857. Imaging support was provided by NIH Grant Nos. P20 RR016454, P30 GM103324–01 and P20 GM103408. Aaron Simmons, Shuai Li and Joshua Sukeena assisted with immunohistochemistry. We would like to thank Rachel Wong and Adam Bleckert for assistance with the colocalization analysis.

REFERENCES

1. Fuerst PG, Bruce F, Tian M, Wei W, Elstrott J, Feller MB, Erskine L, Singer JH, Burgess RW. DSCAM and DSCAML1 function in self-avoidance in multiple cell types in the developing mouse retina. Neuron 2009; 64:484-97. [PMID: 19945391].

2. Yamagata M, Sanes JR. Dscam and Sidekick proteins direct lamina-specific synaptic connections in vertebrate retina. Nature 2008; 451:465-9. [PMID: 18216854].

3. Fuerst PG, Koizumi A, Masland RH, Burgess RW. Neurite arborization and mosaic spacing in the mouse retina require DSCAM. Nature 2008; 451:470-4. [PMID: 18216855].

4. Masland RH. The neuronal organization of the retina. Neuron 2012; 76:266-80. [PMID: 23083731].

5. Hinck L, Nelson WJ, Papkoff J. Wnt-1 modulates cell-cell adhesion in mammalian cells by stabilizing beta-catenin binding to the cell adhesion protein cadherin. J Cell Biol 1994; 124:729-41. [PMID: 8120095].

6. de Andrade GB, Long SS, Fleming H, Li W, Fuerst PG. DSCAM localization and function at the mouse cone synapse. J Comp Neurol 2014; 522:2609-33. [PMID: 24477985].

7. Schramm RD, Li S, Harris BS, Rounds RP, Burgess RW, Ytreberg FM, Fuerst PG. A novel mouse Dscam mutation inhibits localization and shedding of DSCAM. PLoS ONE 2012; 7:e52652-[PMID: 23300735].

8. Fuerst PG, Bruce F, Rounds RP, Erskine L, Burgess RW. Cell autonomy of DSCAM function in retinal development. Dev Biol 2012; 361:326-37. [PMID: 22063212].

9. Fuerst PG, Harris BS, Johnson KR, Burgess RW. A novel null allele of mouse DSCAM survives to adulthood on an inbred C3H background with reduced phenotypic variability. Genesis 2010; 48:578-84. [PMID: 20715164].

10. Soto F, Bleckert A, Lewis R, Kang Y, Kerschensteiner D, Craig AM, Wong RO. Coordinated increase in inhibitory and excitatory synapses onto retinal ganglion cells during development. Neural Dev 2011; 6:31-[PMID: 21864334].

11. Bleckert A, Parker ED, Kang Y, Pancaroglu R, Soto F, Lewis R, Craig AM, Wong RO. Spatial relationships between GABAergic and glutamatergic synapses on the dendrites of distinct types of mouse retinal ganglion cells across development. PLoS ONE 2013; 8:e69612-[PMID: 23922756].

12. Maynard KR, Stein E. DSCAM contributes to dendrite arborization and spine formation in the developing cerebral cortex. J Neurosci 2012; 32:16637-50. [PMID: 23175819].

13. Blank M, Fuerst PG, Stevens B, Nouri N, Kirkby L, Warrier D, Barres BA, Feller MB, Huberman AD, Burgess RW, Garner CC. The Down syndrome critical region regulates retinogeniculate refinement. J Neurosci 2011; 31:5764-76. [PMID: 21490218].

14. Li HL, Huang BS, Vishwasrao H, Sutedja N, Chen W, Jin I, Hawkins RD, Bailey CH, Kandel ER. Dscam mediates remodeling of glutamate receptors in Aplysia during de novo and learning-related synapse formation. Neuron 2009; 61:527-40. [PMID: 19249274].

15. Greferath U, Grunert U, Fritschy JM, Stephenson A, Mohler H, Wassle H. GABAA receptor subunits have differential distributions in the rat retina: in situ hybridization and immunohistochemistry. J Comp Neurol 1995; 353:553-71. [PMID: 7759615].

16. Dick O, Hack I, Altrock WD, Garner CC, Gundelfinger ED, Brandstatter JH. Localization of the presynaptic cytomatrix protein piccolo at ribbon and conventional synapses in the rat retina: Comparison with bassoon. J Comp Neurol 2001; 439:224-34. [PMID: 11596050].

17. Sherry DM, Mitchell R, Standifer KM, du Plessis B. Distribution of plasma membrane-associated syntaxins 1 through 4 indicates distinct trafficking functions in the synaptic layers of the mouse retina. BMC Neurosci 2006; 7:54-[PMID: 16839421].

18. Yamagata M, Sanes JR. Expanding the Ig superfamily code for laminar specificity in retina: expression and role of contactins. J Neurosci 2012; 32:14402-14. [PMID: 23055510].

19. Sernagor E, Eglen SJ, Wong RO. Development of retinal ganglion cell structure and function. Prog Retin Eye Res 2001; 20:139-74. [PMID: 11173250].

20. Chen SK, Chew KS, McNeill DS, Keeley PW, Ecker JL, Mao BQ, Pahlberg J, Kim B, Lee SC, Fox MA, Guido W, Wong KY, Sampath AP, Reese BE, Kuruvilla R, Hattar S. Apoptosis regulates ipRGC spacing necessary for rods and cones to drive circadian photoentrainment. Neuron 2013; 77:503-15. [PMID: 23395376].

21. Suzuki SC, Takeichi M. Cadherins in neuronal morphogenesis and function. Dev Growth Differ 2008; 50:Suppl 1S119-30. [PMID: 18430170].

22. Takeichi M, Abe K. Synaptic contact dynamics controlled by cadherin and catenins. Trends Cell Biol 2005; 15:216-21. [PMID: 15817378].

23. Fu X, Sun H, Klein WH, Mu X. Beta-catenin is essential for lamination but not neurogenesis in mouse retinal development. Dev Biol 2006; 299:424-37. [PMID: 16959241].

24. De la Huerta I, Kim IJ, Voinescu PE, Sanes JR. Direction-selective retinal ganglion cells arise from molecularly specified multipotential progenitors. Proc Natl Acad Sci USA 2012; [PMID: 23045641].

25. Duan X, Krishnaswamy A, De la Huerta I, Sanes JR, Type II. Cadherins Guide Assembly of a Direction-Selective Retinal Circuit. Cell 2014; 158:793-807. [PMID: 25126785].

26. Purohit AA, Li W, Qu C, Dwyer T, Shao Q, Guan KL, Liu G. Down Syndrome Cell Adhesion Molecule (DSCAM) Associates with Uncoordinated-5C (UNC5C) in Netrin-1-Mediated Growth Cone Collapse. J Biol Chem 2012; 287:27126-38. [PMID: 22685302].

Articles are provided courtesy of Emory University and the Zhongshan Ophthalmic Center, Sun Yat-sen University, P.R. China. The print version of this article was created on 10 October 2014. This reflects all typographical corrections and errata to the article through that date. Details of any changes may be found in the online version of the article.